Kinetics of formic acid dehydration on Pt electrodes by time-resolved ATR-SEIRAS

ⒾD Laura Pérez-Martínez, ⒾD Enrique Herrero and ⒾD Angel Cuesta

View Online   Export Citation   CrossMark

ARTICLES YOU MAY BE INTERESTED IN

AIP Publishing

Kinetics of formic acid dehydration on Pt electrodes by time-resolved ATR-SEIRAS

View Online   Export Citation   CrossMark

Laura Pérez-Martínez,[1,a] (iD)   Enrique Herrero,[2] (iD) and Angel Cuesta[1,3,b] (iD)

AFFILIATIONS

[1] School of Natural and Computing Sciences, University of Aberdeen, Aberdeen AB24 3UE Scotland, United Kingdom
[2] Instituto de Electroquímica, Universidad de Alicante, E-03080 Alicante, Spain
[3] Centre for Energy Transition, University of Aberdeen, AB24 3FX Aberdeen, Scotland, United Kingdom

Note: This paper is part of the JCP Special Topic on Chemical Physics of Electrochemical Energy Materials.
[a] Current address: AIJU, Avda. de la Industria 23, E-03440 Ibi, Alicante Spain.
[b] Author to whom correspondence should be addressed: angel.cuestaciscar@abdn.ac.uk

ABSTRACT

The potential dependence of the rate of dehydration of formic acid to adsorbed CO (CO_{ad}) on Pt at pH 1 has been studied on a polycrystalline Pt surface by time-resolved surface-enhanced infrared absorption spectroscopy in the attenuated total reflection mode (ATR-SEIRAS) with simultaneous recording of current transients after a potential step. A range of formic acid concentrations has been used to obtain a deeper insight into the mechanism of the reaction. The experiments have allowed us to confirm that the potential dependence of the rate of dehydration has a bell shape, going through a maximum around the potential of zero total charge (pztc) of the most active site. The analysis of the integrated intensity and frequency of the bands corresponding to CO_L and $CO_{B/M}$ shows a progressive population of the active sites on the surface. The observed potential dependence of the rate of formation of CO_{ad} is consistent with a mechanism in which the reversible electroadsorption of $HCOO_{ad}$ is followed by its rate-determining reduction to CO_{ad}.

I. INTRODUCTION

The study of the formic acid oxidation reaction (FAOR) on platinum is a popular research topic in electrocatalysis that has received much interest and attention for a long time.[1,2] This is because the formic acid oxidation is the simplest electrocatalytic reaction involving an organic molecule (only two electrons and two protons need to be transferred for its complete oxidation to CO_2), and it can, therefore, be seen as a model reaction to understand the mechanism of more complex reactions such as methanol oxidation.[3–6] Furthermore, formic acid can be used as fuel in direct formic acid fuel cells (DFAFCs).[7,8] It is well known that the FAOR proceeds on Pt through a dual-path mechanism, first proposed by Capon and Parsons back in 1973,[9] composed of a direct path that leads directly to the formation of CO_2, and an indirect path through a poisoning intermediate, namely, adsorbed CO (CO_{ad}).[10,11]

Some years ago, our group demonstrated that adsorbed formate ($HCOO_{ad}$) is the bifurcation point in the dual-path mechanism,

the last intermediate common to both paths (see Scheme 1).[11,12] This very important conclusion has been discussed, analyzed, and confirmed by our and other research groups during the last ten years.[13–16]

Formate can be adsorbed through either one or both of its oxygen atoms (mono- and bidentate adsorbed formate, respectively). Bi- and monodentate adsorbed formates should be expected to be in equilibrium with each other on the electrode surface, although the equilibrium is strongly displaced to the bidentate form, which is the most stable of these configurations and the only one that has been detected on electrode surfaces.[11,17–20] The bidentate adsorbed formate was initially proposed to be the reactive intermediate in the direct path,[21] but this has been disproved because the H atom is far from the surface and, thus, the kinetic barrier for the cleavage of the C–H bond is very high.[20,22] The strong evidence that some form of $HCOO_{ad}$ must still be the reactive intermediate in the direct path of the FAOR[14,15,23–27] has led to the current consensus that the monodentate adsorbed formate is the actual reaction intermediate. Although the bidentate form can block sites on the
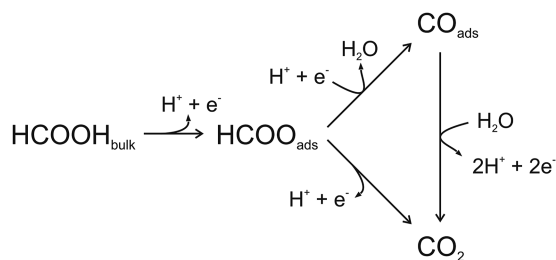
SCHEME 1. The dual path mechanism for the electrocatalytic oxidation of formic acid, where adsorbed formate is the last intermediate common to both paths.

electrocatalyst surface needed for the reaction to proceed, it is not a dead end, as it can act as a reservoir of monodentate adsorbed formate through the chemical equilibrium connecting the two forms and can stabilize the H-down form of neighboring monodentate adsorbed formates.[14,28–30]

In the so-called indirect path, CO_{ad} was very early identified as the catalytic poison.[10,31–33] CO_{ad} forms around a quite narrow potential range of about 100 mV around the local point of zero total charge (pztc).[11,34] Although the rates of CO_{ad} formation are significantly slower than those of the direct path,[14] from a practical perspective, the buildup of CO_{ad} results in a considerable decrease in the DFAFC's power and efficiency because it can be removed only at high overpotentials. The study of the mechanism of its formation can provide the information required to engineer electrocatalysts on which CO_{ad} formation is inhibited. Our group has shown that a minimum of three contiguous Pt atoms are required for the dehydration of HCOOH on Pt,[19] and later, we provided spectrokinetic evidence using time-resolved surface-enhanced infrared absorption spectroscopy in the attenuated total reflection mode (ATR-SEIRAS) that $HCOO_{ad}$ is also the intermediate in the indirect path and, therefore, the last intermediate common to both paths in the reaction mechanism (see Scheme 1).[11,12]

Recent pulsed-voltammetry studies of the kinetics of the direct and indirect pathways of formic acid oxidation on Pt(111) and Pt(100)[15,16] confirm, in agreement with Grozovski *et al.*[34] and previous predictions,[11] that the rate of dehydration of formic acid depends on the applied potential and goes through a maximum and that the rate of poisoning by CO_{ad} on Pt(111) is much slower than on Pt(100), as expected from the difference between their pztc's.[11] The more positive pztc on Pt(111) implies that more positive potentials, at which the rate constant for the reduction of $HCOO_{ad}$ to CO_{ad} is smaller, are needed to have a sufficiently high coverage of $HCOO_{ad}$. On the contrary, on Pt(100), sufficiently high coverages of $HCOO_{ad}$ can be reached at more negative potentials, at which the rate constant for the reduction of $HCOO_{ad}$ to CO_{ad} is larger and the buildup of CO_{ad} happens faster.[15]

We have also recently studied the oxidation of methanol to CO_{ad} on Pt using the high sensitivity and the absence of transport limitations offered by ATR-SEIRAS,[35] which allowed us to monitor in real-time the evolution of the CO_{ad} coverage (θ_{CO}). Our results allowed us to infer which sites on the Pt surface are the active ones in which potential region for the methanol dehydrogenation reaction and provided Tafel plots that revealed the effect of adsorbed spectator species on the reaction rate. Following the same methodology,

we present here a detailed study that combines chronoamperometry with time-resolved ATR-SEIRAS. These experiments have allowed us to carefully monitor the progressive population of CO_{ad} on the Pt surface at pH 1 as a function of potential and formic acid concentration. These results are compared with those recently obtained for methanol dehydrogenation[35] and discussed within the context of our recent results using pulsed voltammetry.[15,16]

II. EXPERIMENTAL PART

Electrolytes were prepared by dissolving $HClO_4$ (70%, Merck p.a. EMSURE) in ultrapure water (Milli-Q) up to a concentration of 0.1M (approximate pH 1). The solutions containing formic acid (Sigma-Aldrich ≥ 98%) were prepared by adding it to the desired concentration (8×10^{-3}, 4×10^{-3}, 2×10^{-3}, 10^{-3}, and 5×10^{-4}M). All the experiments were performed using N_2 purging at room temperature. A flame-annealed Pt wire (Alfa Aesar, 99.997% metals basis) was used as a counter electrode and a homemade Ag/AgCl (KCl_{sat}) electrode as a reference. However, all the potentials in the text are referred to the reversible hydrogen electrode (RHE) unless otherwise stated. The working electrode was a Pt film deposited following a previously reported procedure[21] on the totally reflecting plane of a Si prism beveled at 60°.

The ATR-SEIRA spectra were recorded using a Nicolet iS50R FTIR spectrometer equipped with a liquid nitrogen-cooled MCT detector and a homemade ATR accessory, using unpolarized light. A new reference spectrum was recorded before each spectral series at 0.96 V vs RHE. This potential was chosen for the background spectrum because it is positive enough to have any present CO_{ad} oxidized before starting the experiment[17,36] while minimizing changes in the baseline of the spectra. Differential spectra are reported in absorbance units (a.u.), calculated as $-\log\left(\frac{R_{sample}}{R_{reference}}\right)$, where $R_{reference}$ and R_{sample} are the reference and sample spectra, respectively. The positive bands correspond to species present in the sample spectrum that were absent or present at a lower concentration in the reference spectrum, while the negative bands correspond to species present in the reference spectrum that are absent or present at a lower concentration in the sample spectrum. A series of differential spectra after a potential step were obtained in the kinetics mode by accumulating 1 interferogram per spectrum with a spectral resolution in the range between 4 and 32 cm^{-1}. An adequate combination of these two parameters allowed for achieving a time resolution high enough to monitor the speed of the CO_{ad} band growth with a good signal-to-noise ratio for each specific experiment. The specific parameters used in each of the experiments presented in this work are provided in the corresponding figure captions. The Si prism where the working electrode is deposited was attached to the spectroelectrochemical cell using an O-ring seal, and electrical contact with the film was made by pressing onto it a circular platinum wire. Before any IR measurements, the film was cycled in the corresponding electrolyte to check its stability and then rinsed with Milli-Q water before filling the cell with the solution containing the target concentration of formic acid.

III. RESULTS AND DISCUSSION

Figure 1(a) shows the cyclic voltammogram (CV) of polycrystalline Pt in 0.1M $HClO_4$ within the potential range between
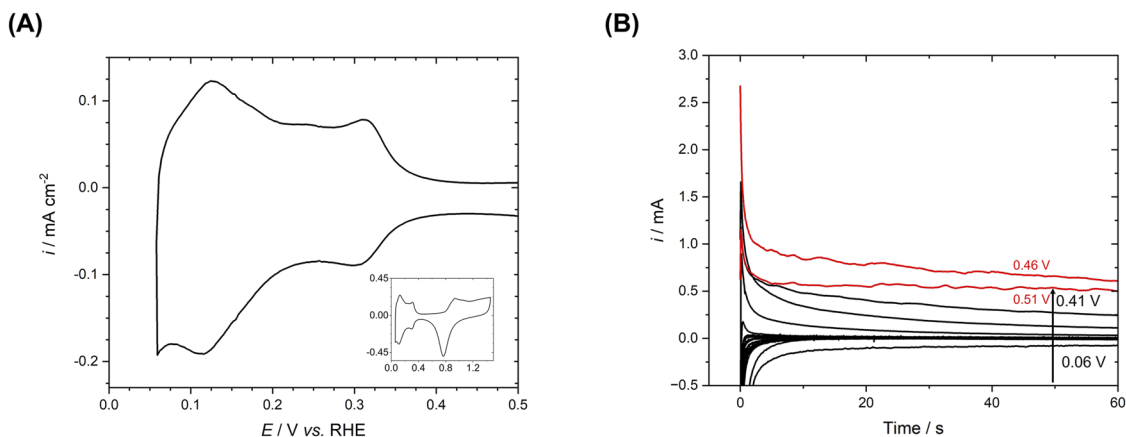
FIG. 1. (a) Zoom into the region between 0.05 and 0.5 V of the cyclic voltammogram of a polycrystalline Pt electrode in 0.1M HClO$_4$ at 0.05 V s^{-1}, which corresponds to the potential region where the formation of CO$_{ad}$ was monitored using the time-resolved ATR-SEIRAS. The whole CV is shown in the inset. (b) Characteristic current transients recorded simultaneously with an ATR-SEIRA spectral series in 2×10^{-3}M HCOOH solutions in 0.1M HClO$_4$ after a potential step from 0.96 V to selected potentials within this region.

0.05 and 0.46 V, which encompasses the H$_{upd}$ region plus the negative end of the double-layer region. Characteristic chronoamperometric transients recorded simultaneously with the time-resolved ATR-SEIRA spectra in the presence of 2×10^{-3}M HCOOH after a potential step from 0.96 V to selected potentials within this potential region are presented in Fig. 1(b).

Despite not involving any net electron transfer, the rate of the dehydration of formic acid to CO$_{ad}$ on Pt,

$$\text{HCOOH} \rightarrow \text{CO}_{ad} + \text{H}_2\text{O}, \qquad (1)$$
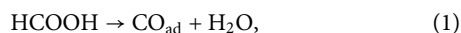
has been known for decades to be potentially dependent. As we have shown,[11,12] this potential dependence of a purely chemical reaction can be explained if a two-step electrochemical mechanism is followed, in which an oxidative reversible electroadsorption,

$$\text{HCOOH} \leftrightharpoons \text{HCOO}_{ad} + \text{H}^+ + e^-, \qquad (2)$$
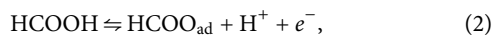
is followed by the rate-determining reduction of formate (which may, and most likely does, occur in more than one elementary step),

$$\text{HCOO}_{ad} + \text{H}^+ + e^- \rightarrow \text{CO}_{ad} + \text{H}_2\text{O}, \qquad (3)$$

Because this reaction sequence leads to a zero net electron transfer, the rate of this reaction cannot be determined directly from electrochemical experiments, although it can be indirectly determined from the decay of the current corresponding to either the formic acid oxidation reaction (FAOR) or the hydrogen evolution reaction (HER) at the selected potential using an appropriate kinetic model.[13,15,20,34] The extrapolation of the so-obtained rate of formation of CO$_{ad}$ to $t = 0$ leads to the intrinsic rate of poisoning of the catalyst, i.e., corresponding to zero CO$_{ad}$ coverage (θ_{CO} = 0). This extrapolation is, however, not free from interference, as the current measured will contain contributions from double-layer charging, the reduction of the PtO$_x$ layer created at the initial potential, and the adsorption and then CO$_{ad}$-induced desorption of H$_{upd}$.[35]

The transients in Fig. 1(b) all show a continuous current decay, clear evidence of self-poisoning due to the buildup of CO$_{ad}$. At 0.51 V, on the contrary, after an initial decay, a constant current is reached, which suggests that a stationary state has been reached at which θ_{CO} remains constant because it is being oxidized at the same rate at which it is being formed. The shape of the transient at 0.46 V suggests that it also tends toward a steady state, but our experiment was not long enough for that steady state to be reached. The noisy transients at both 0.46 and 0.51 V (and, to a lesser extent, also at 0.41 V) suggest a mixed kinetic-transport controlled oxidation of formic acid (experiments were performed while bubbling N$_2$ through the solution). The current is higher at 0.46 than at 0.51 V because (i) the steady state at the former potential has not been reached and (ii) 0.51 V is located after the peak potential in the oxidation of formic acid (see CVs in Refs. 15 and 16 and the discussions therein).

In contrast to the limitations in the study of these current transients, the high time resolution achievable with ATR-SEIRAS allows us to follow the growth of the infrared CO$_{ad}$ bands after a potential step and to extrapolate the rate of CO$_{ad}$ formation to $t = 0$ without interference from any other process. We have recently demonstrated how powerful this approach can be and the wealth of information that can be gathered from this kind of experiment in the case of the oxidation of methanol to CO$_{ad}$ on Pt electrodes.[35] As shown there, with the time resolution achieved in our ATR-SEIRAS experiments, the recording of the time evolution of the CO$_{ad}$ bands in the spectral series starts once the interfacial potential profile has been properly established and is, therefore, an accurate reflection of the kinetics of the dehydration reaction at the corresponding applied potential.

Figure 2(a) shows a typical time-resolved ATR-SEIRA spectral series recorded after a potential step from 0.96 to 0.11 V in 0.1M HClO$_4$ containing 2×10^{-3}M HCOOH with a time interval of 0.15 s. Please note that $t = 0$ corresponds to the last spectrum in the series just before the first observation of a CO$_{ad}$ band. The spectra separated by 0.3 s are shown as a representative sample of those recorded
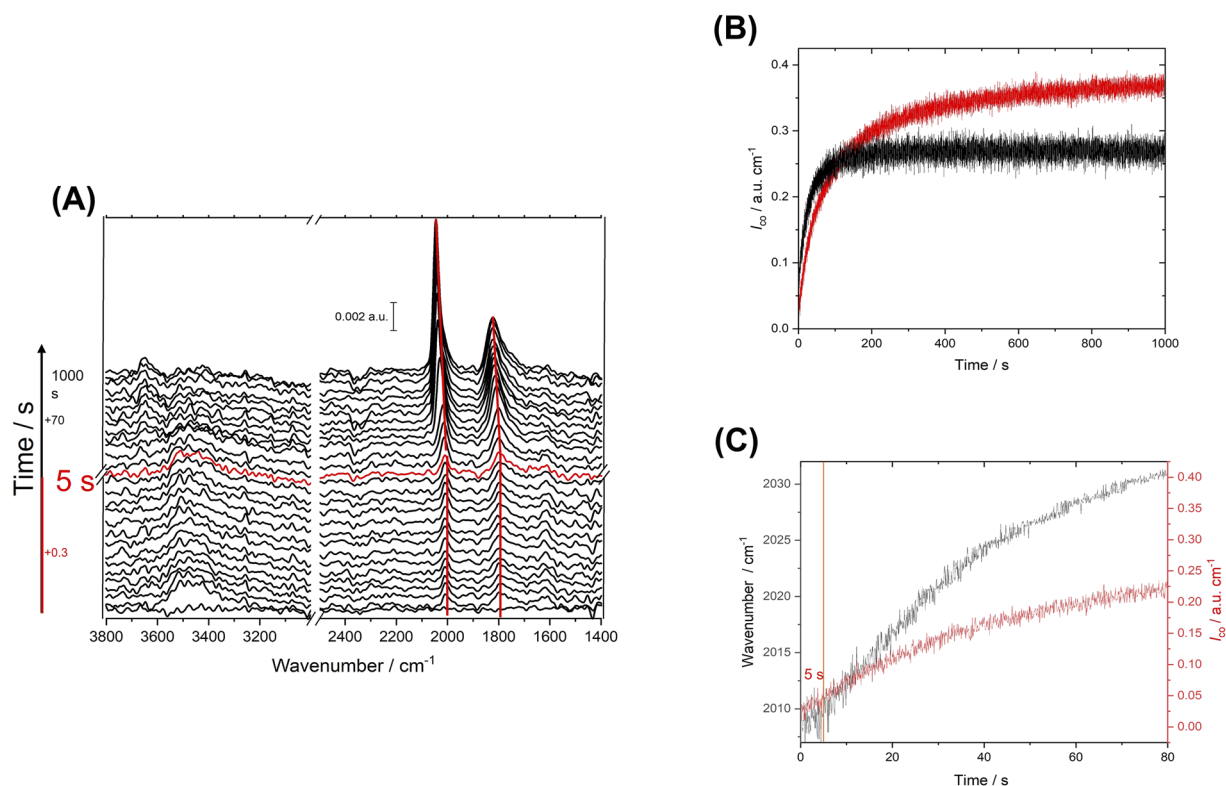
FIG. 2. (a) A typical time-resolved ATR-SEIRA spectral series showing the buildup of CO_{ad} on Pt in 0.1M $HClO_4$ containing 2×10^{-3}M HCOOH, recorded after a potential step from 0.96 to 0.11 V vs RHE. Each spectrum consists of a single interferogram recorded with a spectral resolution of 16 cm^{-1}, resulting in a time interval between spectra of 0.15 s. The reference spectrum was taken at 0.96 V. Only selected spectra are shown. Between 0 and 5 s (red spectrum), a spectrum every 0.3 s is shown, whereas from that point onwards, a spectrum every 70 s is shown. (b) Time dependence of I_{CO_L} (red) and $I_{CO_{B/M}}$ (black) during the whole experiment. (c) Time evolution of the stretching frequency of CO_L (black line) and of I_{CO_L} (red line) during the first 80 s.

during the first 5 s, while the spectra separated by intervals of 70 s have been selected for the period between 5 and 1000 s.

The characteristic bands corresponding to the C–O stretching of linearly adsorbed CO (CO_L, appearing initially at 2010 cm^{-1}) and to bridge-bonded (CO_B) plus multiply-bonded (CO_M) adsorbed CO (the very asymmetric band initially appearing at 1790 cm^{-1}) are clearly visible in the spectra. For the sake of simplicity and following Yan $et~al.$,[37] CO_M and CO_B will be considered jointly ($CO_{B/M}$) when integrating the band intensity for analysis of the rate of formation of CO_{ad}.

As expected, the integrated intensity of both CO_L (I_{CO_L}, red) and $CO_{B/M}$ ($I_{CO_{B/M}}$, black) increases with time until they reach a constant value when the maximum θ_{CO} is reached ($I_{CO_{B/M}}$ reaches its maximum value at shorter times). Due to dipole–dipole coupling between neighboring adsorbed oscillators,[38,39] the continuously decreasing distance between oscillating CO_{ad} dipoles as θ_{CO} increases should lead to a continuous increase in the CO-stretching frequency parallel to the increase in the integrated absorbance [shown in Fig. 2(c) for CO_L]. However, the frequency of the CO_L band remains constant within our experimental error during the first 5 s [the vertical lines in Fig. 2(a) show that this is true both for CO_L and CO_B], although the integrated absorbance increases during this

time. This suggests that, during this initial 5 s, θ_{CO} is low enough for the surface to accommodate the newly formed CO_{ad} without a significant decrease in the distance between oscillating dipoles. This result is in good agreement with our recent work on the dehydrogenation of methanol on Pt, where the frequency was found to grow in a staircase manner with time too during the initial stages of CO_{ad} buildup. However, in that case, the rate of CO_{ad} growth was slower, and more than one period of constant or nearly constant frequency, despite continuous growth in θ_{CO}, could be observed.[35] In addition, contrary to what we observed during the oxidation of methanol to CO_{ad} on Pt electrodes,[35] the CO_L band shows a clear inhomogeneous broadening already in the first spectrum recorded, suggesting that more than one kind of adsorption sites have already been occupied after 0.1 s.[38,39]

The derivative of the spectroscopic transient (i.e., of the time dependence of the integrated absorbance of the CO_L and $CO_{B/M}$ bands) provides a direct measure of the rate of formation of CO_{ad}. Because the product of the reaction (CO_{ad}) blocks sites on the surface, any kinetic study must be based on the rate of formation of CO_{ad} at $t = 0$, when all the surface is active, which can be obtained by extrapolating the derivative of the spectroscopic transients to $t = 0$. Figure 3 shows plots of the time evolution of I_{CO_L} (red), $I_{CO_{B/M}}$
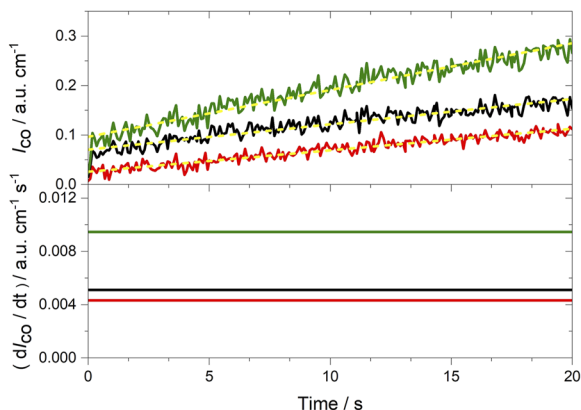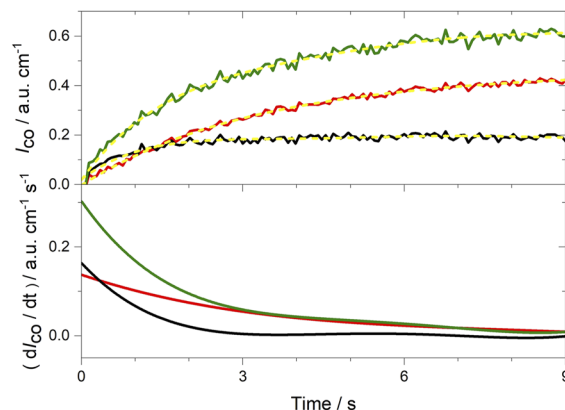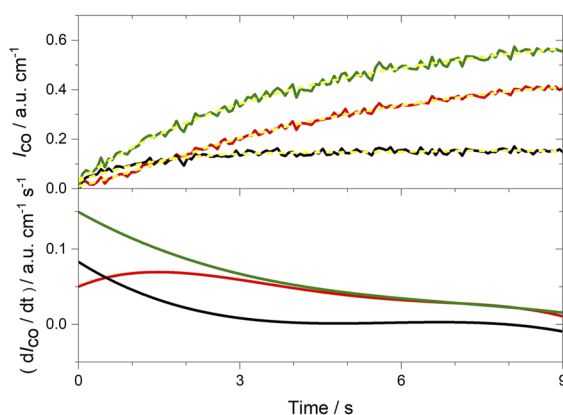
FIG. 3. Time dependence of I_{CO_L} (red), $I_{CO_{B/M}}$ (black), and $I_{CO_L} + I_{CO_{B/M}}$ (green) (top panels) and of the corresponding derivatives with respect to time (lower panels) obtained from a series of time-resolved ATR-SEIRA spectra in 0.1M HClO$_4$ containing 2×10^{-3}M HCOOH, recorded after a potential step from 0.96 to 0.11 (top left), 0.21 (top right), and 0.26 V (bottom). The integrated intensity vs time data were smoothed by fitting to a fifth-order polynomial, and the result of the fit (dotted yellow lines) was used to obtain the derivatives in the bottom panels.

(black), and $(I_{CO_L} + I_{CO_{B/M}})$ (green), as well as the time dependence of the corresponding derivatives with respect to time ($\frac{dI_{CO_L}}{dt}$, $\frac{dI_{CO_{B/M}}}{dt}$, and $\frac{d(I_{CO_L} + I_{CO_{B/M}})}{dt}$, respectively), obtained at 0.11, 0.21, and 0.26 V from a series of time-resolved ATR-SEIRA spectra in 0.1M HClO$_4$ containing 2×10^{-3}M HCOOH.

As we have discussed recently,[35] when analyzing the rate of CO$_{ad}$ formation at short times, θ_{CO} needs to be estimated from the integrated intensities of both CO$_L$ and CO$_{B/M}$, because at this initial reaction stages, $I_{CO_{B/M}}$ and I_{CO_L} are similar, and at some potentials, CO$_{B/M}$ is the only band present in the spectra. Ignoring this band when analyzing the rate of CO$_{ad}$ formation could, therefore, lead to a considerable error. This can be clearly seen in the results at 0.26 V reported in Fig. 3, where $\frac{dI_{CO_L}}{dt}$ (red line) is seen to initially increase until a maximum is reached, after which it slowly decreases to zero. If CO$_L$ is used as a proxy for the total θ_{CO}, the wrong and

unreasonable conclusion would be reached that, in the initial stages of the reaction, increasing θ_{CO} results in an increase in the surface activity for the dehydration of formic acid. This can be avoided if the sum of the two observable bands and the corresponding derivative, $\frac{d(I_{CO_L} + I_{CO_{B/M}})}{dt}$, are used instead (Fig. 3, green lines). The fact that, under certain conditions, the rate of the reaction is seen to initially remain constant for a relatively long time suggests that, during this time, θ_{CO} remains low enough so as to have a negligible blocking effect. In other words, it is a confirmation that we are analyzing the kinetics of the reaction when θ_{CO} is extremely low.

The same analysis as shown in Fig. 3 has been performed at each applied potential with all the different concentrations of formic acid (data provided in the supplementary material, Figs. S1–S5), and the results have been used to plot the dependence of the rate of formic acid electrooxidation on the potential at several concentrations of HCOOH (Fig. 4).
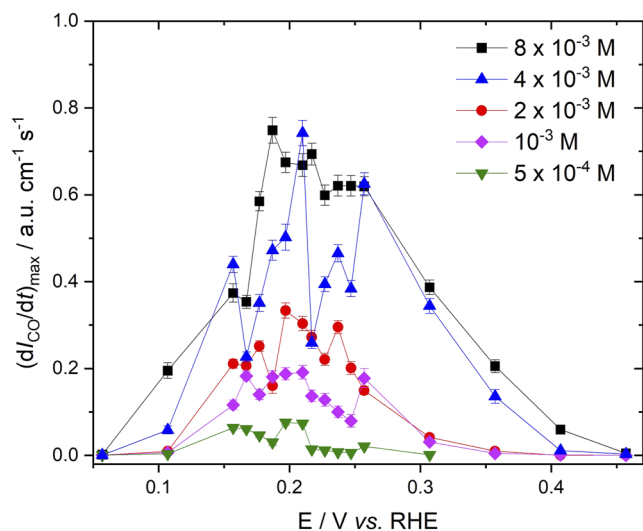
FIG. 4. Potential dependence of the rate of dehydration of HCOOH on Pt calculated by extrapolating to $t = 0$ the derivate of $I_{CO_L} + I_{CO_{B/M}}$ at different concentrations of formic acid (ranging between 5×10^{-4} and 8×10^{-3}M, as indicated in the figure) in 0.1M HClO$_4$. Note that the error bars do not correspond to the standard deviation within a set of similar experiments but to the uncertainty in the rate of dehydration obtained by extrapolation at $t = 0$, due to the noise present in the integrated intensity vs time curves.

The dependence of the rate of dehydration of formic acid on the potential has a bell shape, with a maximum of around 0.2 V, in good agreement with previous work.[15,16,34]

As discussed in previous work,[11] the potential at which the rate of dehydration is maximum corresponds to the point where the product of the formate coverage (θ_{HCOO}) times the rate constant of reaction (3), k_3, is maximum and must, therefore, be associated with the potential of zero total charge (pztc) of the active site. As also discussed previously, because the value of k_3 at any given potential can be expected to depend weakly on the atomic structure of the active site, but θ_{HCOO} at any potential and any concentration will be higher on the site with the most negative pztc, the rate of CO$_{ad}$ formation at the maximum is also the higher the more negative the pztc is. The pztc of Pt(111) is more positive than that of Pt(100), which is more positive than that of Pt(110).[40–43] It is, therefore, not surprising that the maximum rate of formation of CO$_{ad}$ in Fig. 4 is around 0.2 V for all concentrations, which is closer to the pztc of (110)-oriented defect sites than to that of (100)-oriented sites and far away from the pztc of (111) sites. The contributions from one-dimensional and small two-dimensional (100)-oriented sites are expected to be around 0.3 V, while dehydration on larger two-dimensional (100)-oriented sites is expected to emerge around 0.4 V. These two contributions lead to the broadening of the peak in Fig. 4 with increasing HCOOH concentration. However, the negative shift of the potential at which the rate of formic acid dehydration is maximum with increasing HCOOH concentration, expected for the reaction mechanism composed of reactions (2) and (3)[11] and recently observed when the reaction is catalyzed by Pt(100) electrodes,[15] cannot be observed in Fig. 4, which shows a broad maximum between 0.15 and 0.2 V for all but the two lowest concentrations of HCOOH. The potential at

which the rate of dehydration of formic acid on polycrystalline Pt reaches its maximum coincides very well with the completion of the first peak in the hydrogen adsorption region of the CV (see Fig. 1), which suggests that the observed lack of dependence of the position of the maximum on the HCOOH concentration is due to the overlap on (110)-oriented defect sites of the adsorption of formate with that of hydrogen. It should be noted that the peak potential for this peak should be almost independent of the formate concentration since the peak potential is almost identical in perchloric and sulfuric acid solutions (sulfate and formate adsorb similarly strongly on Pt).

At concentrations higher than 2×10^{-3}M, the rate of dehydration in the potential region between 0.2 and 0.3 V [the latter corresponding to the second peak in the hydrogen region of the CV and attributed to the desorption of hydrogen from (100)-oriented sites] grows faster than at $E < 0.2$ V. We attribute this behavior to the contribution of (100)-oriented sites to the reaction. Because the potential at which the rate of dehydration is maximum on these sites will shift negatively with increasing HCOOH concentration,[15] the contribution of these sites is responsible for the broadening of the peak in Fig. 4 as the concentration of formic acid increases.

Assuming that the reduction of HCOO$_{ad}$ to CO$_{ad}$ [Reaction (3)] is the rate-determining step and taking into account the site-demanding nature of the formic acid dehydration reaction,[19] the rate equation for the dehydration of formic acid is

$$\frac{d\theta_{CO}}{dt} = k_3 \theta_{HCOO} (1 - \theta_{HCOO} - \theta_H - \theta_{CO}), \qquad (4)$$

However, because the reaction rate in Fig. 4 corresponds to that at $t = 0$, when $\theta_{CO} = 0$, Eq. (4) reduces to

$$\frac{d\theta_{CO}}{dt} = k_3 \theta_{HCOO} (1 - \theta_{HCOO} - \theta_H). \qquad (5)$$

Assuming that the adsorption of formate, reaction (2), obeys the Langmuir isotherm, and taking into account that formic acid dehydration occurs mostly within the hydrogen adsorption region, the coverage of formate will be given by

$$\theta_{HCOO} = \frac{k_2 c_{HCOOH} (1 - \theta_H)}{k_{-2} + k_2 c_{HCOOH}}, \qquad (6)$$

where k_2 and k_{-2} are the rate constants of formate adsorption and desorption, respectively. The rate of formation of CO$_{ad}$ from formic acid dehydration on Pt should hence be

$$\frac{d\theta_{CO}}{dt} = k_3 \frac{k_2 c_{HCOOH} (1 - \theta_H)}{k_{-2} + k_2 c_{HCOOH}} (1 - \theta_{HCOO} - \theta_H) \qquad (7)$$

(note that because the pH is constant throughout the experiment, both k_{-2} and k_3 contain the term corresponding to the H$^+$ concentration, c_{H^+}).

At potentials at which either θ_H or θ_{HCOO} are very high, the rate of dehydration should be very small and approach zero at any HCOOH concentration, as is, indeed, the case in Fig. 4 at both the negative and positive potential ends of the plot. At any other potential, the dependence of the reaction rate on the formic acid concentration will be complex. However, at potentials at which θ_H and θ_{HCOO} remain constant [as expected between the two peaks in the hydrogen adsorption region of Pt, where replacement of H$_{ad}$ by
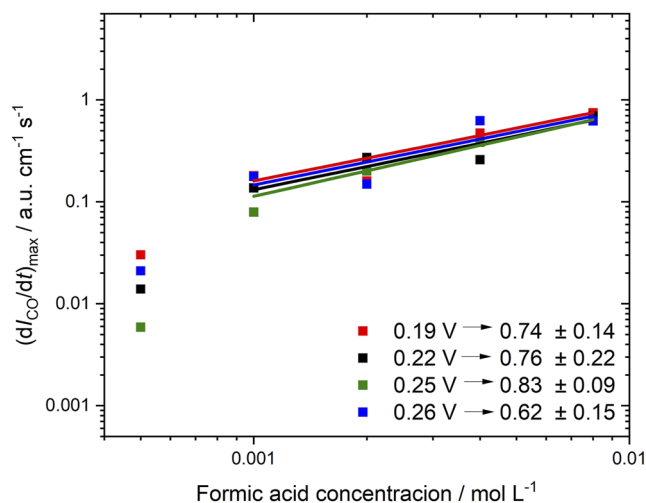
FIG. 5. Double logarithmic plot of the dependence on the formic acid concentration of the rate of dehydration of HCOOH to CO_{ad} on Pt at $t = 0$ within the potential region between 0.19 and 0.26 V. The values in the legend correspond the slope at the indicated potential in the linear region of the plot.

$HCOO_{ad}$ on (110)-oriented defects must be complete but has barely started yet on (100)-oriented sites], the reaction is expected to be first order with respect to the formic acid concentration as long as $k_2 c_{HCOOH} \ll k_{-2}$. As shown in Fig. 5, this seems to be, indeed, the case between 0.19 and 0.26 V, although at the lowest concentration used, the experimental data clearly deviate from the trend at higher concentrations.

IV. CONCLUSIONS

The high sensitivity and the absence of transport limitations characteristic of ATR-SEIRAS have permitted us to follow in detail the electrocatalytic formation of CO_{ad} from formic acid on platinum. A real-time analysis of the intensity and shape of the CO_{ad} characteristic bands, CO_L and $CO_{B/M}$, and of their corresponding derivatives has enabled us to study the rate of formation of CO_{ad} as well as its dependence on potential at constant concentration and concentration at a constant potential. The comparative analysis of the time evolution of both the integrated intensity and the frequency of the bands corresponding to CO_L and $CO_{B/M}$ suggests a progressive population by CO_{ad} of the active sites on the surface.

The time-resolved spectra recorded simultaneously with current transients after a potential step in the H_{upd} region have confirmed the relationship between the potential of zero total charge (pztc) of the active site and the rate of dehydration of formic acid. In agreement with previous works,[15,16] the rate of dehydration has a bell-shaped dependence on the potential and goes through a broad maximum extending between 0.15 and 0.2 V whose position is independent of the formic acid concentration. This is due to the polycrystalline nature of the platinum film, which contains a large multiplicity of sites, each with its own pztc, but is dominated by (110) and (100) defect sites. In addition, a kinetic mechanism depending on the potential and θ_H, θ_{HCOO}, and θ_{CO} has been proposed where the reaction would be expected to be first order with respect to the formic acid concentration when $\theta_{CO} \approx 0$, θ_H, and θ_{HCOO} are approximately constant, and $k_2 c_{HCOOH} \ll k_{-2}$.

These results provide additional support to the proposal that $HCOO_{ad}$ is the crucial intermediate in the electro-oxidation of HCOOH.

SUPPLEMENTARY MATERIAL

See the supplementary material for Figs. S1–S5.

AUTHOR DECLARATIONS

Conflict of Interest

The authors have no conflicts to disclose.

Author Contributions

The manuscript was written through contributions of all authors. All authors have given approval to the final version of the manuscript.

Laura Pérez-Martínez: Formal analysis (lead); Investigation (lead); Methodology (equal); Writing – original draft (lead); Writing – review & editing (equal). **Enrique Herrero**: Formal analysis (equal); Writing – review & editing (equal). **Angel Cuesta**: Conceptualization (lead); Formal analysis (equal); Funding acquisition (lead); Project administration (lead); Resources (lead); Supervision (lead); Writing – review & editing (lead).

DATA AVAILABILITY

The data that support the findings of this study are available from the corresponding author upon reasonable request.

REFERENCES

[1] H. Jahn, Ann. Phys. Chem. **273**, 408 (1889).

[2] F. Salzer, Z. Elektrotech. Elektrochem. **8**, 893 (1902).

[3] E. A. Batista, G. R. P. Malpass, A. J. Motheo, and T. Iwasita, J. Electroanal. Chem. **571**, 273 (2004).

[4] E. A. Batista and T. Iwasita, Langmuir **22**, 7912 (2006).

[5] E. A. Batista, G. R. P. Malpass, A. J. Motheo, and T. Iwasita, Electrochem. Commun. **5**, 843 (2003).

[6] H. Wang, T. Löffler, and H. Baltruschat, J. Appl. Electrochem. **31**, 759 (2001).

[7] C. Rice, S. Ha, R. I. Masel, P. Waszczuk, A. Wieckowski, and T. Barnard, J. Power Sources **111**, 83 (2002).

[8] C. Rice, S. Ha, R. I. Masel, and A. Wieckowski, J. Power Sources **115**, 229 (2003).

[9] A. Capon and R. Parsons, J. Electroanal. Chem. **45**, 205 (1973).

[10] B. Beden, A. Bewick, and C. Lamy, J. Electroanal. Chem. **148**, 147 (1983).

[11] A. Cuesta, G. Cabello, M. Osawa, and C. Gutiérrez, ACS Catal. **2**, 728 (2012).

[12] A. Cuesta, G. Cabello, C. Gutiérrez, and M. Osawa, Phys. Chem. Chem. Phys. **13**, 20091 (2011).

[13] V. Grozovski, F. J. Vidal-Iglesias, E. Herrero, and J. M. Feliu, ChemPhysChem **12**, 1641 (2011).

[14] A. Ferre-Vilaplana, J. V. Perales-Rondón, C. Buso-Rogero, J. M. Feliu, and E. Herrero, J. Mater. Chem. A **5**, 21773 (2017).

[15] A. Betts, V. Briega-Martos, A. Cuesta, and E. Herrero, ACS Catal. **10**, 8120 (2020).

[16] M. J. Salamon, V. Briega-martos, A. Cuesta, and E. Herrero, J. Electroanal. Chem. **925**, 116886 (2022).

[17] Y. X. Chen, A. Miki, S. Ye, H. Sakai, and M. Osawa, J. Am. Chem. Soc. **125**, 3680 (2003).

[18] G. Samjeské, A. Miki, S. Ye, and M. Osawa, J. Phys. Chem. B **110**, 16559 (2006).

[19] A. Cuesta, M. Escudero, B. Lanova, and H. Baltruschat, Langmuir **25**, 6500 (2009).

[20] E. Herrero and J. M. Feliu, Curr. Opin. Electrochem. **9**, 145 (2018).

[21] A. Miki, S. Ye, and M. Osawa, Chem. Commun. **2**, 1500 (2002).

[22] H.-F. Wang and Z.-P. Liu, J. Phys. Chem. C **113**, 17502 (2009).

[23] J. Xu, D. Yuan, F. Yang, D. Mei, Z. Zhang, and Y.-X. Chen, Phys. Chem. Chem. Phys. **15**, 4367 (2013).

[24] J. Joo, T. Uchida, A. Cuesta, M. T. M. Koper, and M. Osawa, Electrochim. Acta **129**, 127 (2014).

[25] J. V. Perales-Rondón, S. Brimaud, J. Solla-Gullón, E. Herrero, R. J. Behm, and J. M. Feliu, Electrochim. Acta **180**, 479 (2015).

[26] S. Brimaud, J. Solla-Gullón, I. Weber, J. M. Feliu, and R. J. Behm, ChemElectroChem **1**, 1075 (2014).

[27] J. Joo, T. Uchida, A. Cuesta, M. T. M. Koper, and M. Osawa, J. Am. Chem. Soc. **135**, 9991 (2013).

[28] J. V. Perales-Rondón, E. Herrero, and J. M. Feliu, Electrochim. Acta **140**, 511 (2014).

[29] R. Rizo, R. M. Arán-Ais, and E. Herrero, Curr. Opin. Electrochem. **25**, 100648 (2021).

[30] A. Cuesta, in *Encyclopedia of Interfacial Chemistry: Surface Science and Electrochemistry*, edited by K. Wandelt (Elsevier, 2018), pp. 620–632.

[31] S. G. Sun, J. Clavilier, and A. Bewick, J. Electroanal. Chem. **240**, 147 (1988).

[32] B. Beden, A. Bewick, and C. Lamy, J. Electroanal. Chem. **150**, 505 (1983).

[33] S. C. Chang, L. W. H. Leung, and M. J. Weaver, J. Phys. Chem. **94**, 6013 (1990).

[34] V. Grozovski, V. Climent, E. Herrero, and J. M. Feliu, Phys. Chem. Chem. Phys. **12**, 8822 (2010).

[35] L. Pérez-Martínez, L. M. Machado de los Toyos, J. J. T. Shibuya, and A. Cuesta, ACS Catal. **11**, 13483 (2021).

[36] Y. Zhu, H. Uchida, T. Yajima, and M. Watanabe, Langmuir **17**, 146 (2001).

[37] Y.-G. Yan, Y.-Y. Yang, B. Peng, S. Malkhandi, A. Bund, U. Stimming, and W.-B. Cai, J. Phys. Chem. C **115**, 16378 (2011).

[38] P. Hollins and J. Pritchard, Prog. Surf. Sci. **19**, 275 (1985).

[39] P. Hollins, Surf. Sci. Rep. **16**, 51 (1992).

[40] N. Garcia-Araez, V. Climent, E. Herrero, J. M. Feliu, and J. Lipkowski, Electrochim. Acta **51**, 3787 (2006).

[41] K. Domke, E. Herrero, A. Rodes, and J. M. Feliu, J. Electroanal. Chem. **552**, 115 (2003).

[42] V. Climent, R. Gómez, and J. M. Feliu, Electrochim. Acta **45**, 629 (1999).

[43] R. Gómez, V. Climent, J. M. Feliu, and M. J. Weaver, J. Phys. Chem. B **104**, 597 (2000).